Significant modification of ^{59}Co hyperfine fields assigned to specific structural changes in sputtered Co/Au and Co/Cu multilayers

C. Christides
Department of Engineering Sciences, School of Engineering, University of Patras, 26110 Patras, Greece and Institute of Materials Science, NCSR ''Demokritos,'' 153 10 Aghia Paraskevi, Attiki, Greece

S. Stavroyiannis and D. Niarchos
Institute of Materials Science, NCSR ''Demokritos,'' 153 10 Aghia Paraskevi, Attiki, Greece

M. Wojcik, S. Nadolski, and E. Jedryka
Institute of Physics, Polish Academy of Sciences, 02-668 Warsaw, Poland
(Received 28 April 1998; revised manuscript received 30 November 1998)

Magnetron sputtered Co/Cu and Co/Au multilayers (MLs) with low-field giant magnetoresistance were grown on SiN_x underlayers. Spin-echo ^{59}Co nuclear magnetic resonance (NMR) spectra reveal an fcc Co layer stacking for the Co/Cu multilayers whereas the Co/Au spectra exhibit a unique profile that cannot be assigned to any of the known bulk crystalline or glassy Co structures. Analysis of the Co/Au superlattice reflections, observed with x-ray diffraction (XRD), indicates that Co layers (d_{Co}) expand significantly relative to close-packed lattice values and provide evidence for a reduced atomic density. The complementary study with XRD and NMR measurements has revealed a metastable Co nanostructure in the as-prepared Co/Au MLs. [S0163-1829(99)00913-3]

I. INTRODUCTION

Since 1985 the evolution of the theory of quantum interference phenomena[1] has led to experiments on ultrathin Au films and compositionally modulated films with alternating Co/Au layers, that have shown[2,3] quantum size effects in the resistivity and magnetoresistance. To observe such quantum interference phenomena high-purity ultrathin single-crystal metal films with atomically flat surfaces or interfaces are required, and gold has been proved to be an ideal material for these studies.[2,4] Thus, experimental evidence of quantum size effects has been established after the observation of oscillations in: (i) the dependence of resistivity in ultrathin, epitaxial gold films on the film thickness[2] and (ii) the indirect exchange coupling in Co/Au(111)/Co epitaxial trilayers.[4] Besides the scientific interest to investigate the involved quantum well states on the spin-polarized quantum size effects at the ferromagnetic/no-magnetic interface[5] a great deal of attention has been focused on the technological applications[6] of the resultant giant magnetoresistance (GMR) effect in GMR reading heads and sensors.

Today, (111) textured multilayers with an fcc modulated structure exhibit the largest GMR effect at room temperature for sputtered[7] Co/Cu multilayers (MLs) while such effect is not reported in sputter-grown Co/Au MLs.[8] In epitaxial Co/Au(111)/Co trilayers the GMR curves and the magneto-optical Kerr effect hysteresis loops[4] exhibit a coercive field (H_c) of about 0.5 kOe that *precludes* GMR applications with epitaxial Co/Au MLs, due to the large magnetocrystalline anisotropy of hcp Co. Comparatively, sputtered fcc Co/Cu MLs with appropriate layer thicknesses exhibit GMR ratios[9] up to 60% at room temperature in contrast to epitaxial Co/Cu MLs which register a much smaller GMR effect, and their magnetic switching field (H_s) is several times larger.[10] Thus, from the current experimental evidence it is difficult to distinguish between several contributions to the GMR which are directly or indirectly linked to the structural properties of the superlattice.[11]

Lately, it was reported[12] that sputter-grown $[Co(1\ nm)/Au(2.5\ nm)]_{30}$ MLs with (111) texture exhibit at ambient conditions a GMR ratio of about 3%, an $H_c=0.01$ kOe and an $H_s=0.03$ kOe, which are an order of magnitude less than the corresponding H_c and H_s values reported previously. Conventional[12] and, unpublished yet, high-resolution (HR) cross-section transmission electron microscopy (TEM) indicate that this result is related[12] to unusual atomic packing inside the Co layers. Thus, a modified cubic Co structure give rise to low-field GMR in the as-prepared Co/Au MLs. The developed Co layering deserves further investigation because it is relating a *kinetically* grown Co layer structure with possible GMR applications of Co/Au MLs.

Spin-echo ^{59}Co nuclear magnetic resonance (NMR) has proved[6] to be a powerful method that distinguishes the components from the interfaces and the bulk Co layer[13] and provides information about the local Co atomic packing in multilayered structures. Since the NMR spectra of sputtered GMR Co/Cu MLs have been studied extensively,[6,13] resulting in a unique assignment between the spectral lines and the corresponding Co stacking, we decided to investigate the ^{59}Co NMR spectra of these, low-field GMR, Co/Au MLs in comparison with spectra obtained from Co/Cu MLs as well. In this study, our intent is to probe indirectly the local structure differences in the Co layers of low-field GMR Co/Cu and Co/Au MLs as a function of Co layer thickness (t_{Co}) by using complementary information from ^{59}Co NMR and XRD measurements.

II. EXPERIMENTAL DETAILS

Metallic disks of 99.99% pure elements with diameter 5 cm were used as target materials in a high-vacuum Edwards E360A sputtering system with a cluster of ATOM-TECH

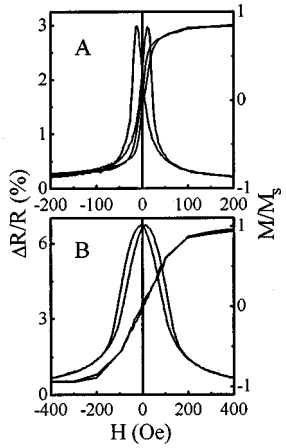

FIG. 1. Isothermal loops of the reduced magnetization M/M_s with the magnetic field applied in-plane, and the corresponding GMR loops measured at 300 K, for (A) the $[Co(1\ nm)/Au(2.5\ nm)]_{30}$ and (B) the $[Co(1\ nm)/Cu(2\ nm)]_{30}$ MLs. For a detailed study, see Refs. 7 and 9.

320-SE balanced magnetron sputter sources. Two series of ML's, with a layer sequence of $[Co(t_{Co})/Au(2.5\ nm)]_{30}$ and $[Co(t_{Co})/Cu(2.1\ nm)]_{30}$, were deposited on top of 100-nm-thick, thermally grown, SiN_x buffer layer on 600-μm-thick Si (100) substrates. During deposition, the Si(100)/ SiN_x substrates were thermally isolated from the water-cooled supporting table. All samples were deposited in a cryogenically pumped chamber with base pressure of 6×10^{-7} Torr under an Ar (99.999% pure) pressure of 3 mTorr. An rf magnetron gun operating at 30 W with a deposition rate of 0.09 nm/s was used for Co, and dc sputtering at 5 W for Au, resulting in a rate of 0.12 nm/s. Determination of the thickness of the various layers was based on the deposition time assuming constant deposition rates. The x-ray-diffraction (XRD) spectra were collected with a SIEMENS D500 powder diffractometer in θ–2θ scans, using Cu-Kα radiation at ambient temperature. Thus, GMR Co/Cu and Co/Au MLs with values of t_{Co} varying between 0.6 and 3.2 nm, and constant $t_{Cu}=2.1$ nm and $t_{Au}=2.5$ nm, respectively, were grown under the same deposition conditions. These deposition conditions and the used substrate were found[12,14] to produce microstructural modifications in the Co layering, inducing low hysteresis (Fig. 1) in the observed GMR curves.

The ^{59}Co NMR experiment was performed at 4.2 K, using an automated, phase sensitive spectrometer.[15] The spin-echo amplitude was recorded every 1 MHz in the frequency range 50–250 MHz, in zero external field. All the spectra are corrected for the enhancement factor variation at each frequency and represent a ^{59}Co hyperfine field distribution in the sample. The hyperfine field B_{hf} can be obtained from the frequency f using the relation $2\pi f=\gamma B_{hf}$, where γ is the ^{59}Co nuclear gyromagnetic ratio ($\gamma/2\pi=10.054$ MHz/T).

III. XRD SPECTRA AND SUPREX ANALYSIS

The Co/Cu XRD spectra are characterized by an intense fcc (111) Co (Cu) peak and a weak (200) fcc peak, indicating that the MLs have strong (111) texture. However, the Co/Cu interfaces give a small x-ray contrast because Co and Cu have similar x-ray atomic scattering factors. Thus superlattice peaks did not appear near the (111) Bragg peak of Co/Cu MLs while in the Co/Au MLs more than six satellite peaks were observed. The low-angle XRD patterns exhibit two Bragg reflections for Co/Cu and four to six Bragg reflections for Co/Au MLs. A thorough examination of the structural, magnetotransport and optical properties of the Co/Cu specimens is given elsewhere.[14] For the Co/Cu MLs the estimated t_{Co} values, obtained from x-ray reflectivity spectra,[14] are 0.78, 1.26, 1.74, 2.37, and 3.12 nm while a $t_{Cu}\approx2.1$ nm is found for all the samples. In Co/Au MLs the layer thicknesses were estimated by fitting the measured XRD intensities with the Superlattice Refinement (SUPREX) program.[16,17] The resultant t_{Co} values are 1.23, 1.56, 2.05, 2.46, and 3.17 nm while a $t_{Au}\approx2.4$ nm is found in all the Co/Au samples.

Since the collected low-angle profiles were not reliable for quantitative analysis only the medium- (MAS) and high-angle satellite (HAS) peaks were used in SUPREX analysis. From the satellite peak positions the average lattice (overall) spacing $\bar{d}=\Lambda/(N_{Co}+N_{Au})$, with N_{Co} and N_{Au} the number of atomic planes of Co and Au in one bilayer, and the bilayer thickness $\Lambda=t_{Co}+t_{Au}+t'$ ($t'=$total interface thickness) can be determined directly. Every crystalline layer is described by N atomic planes which are separated by a lattice constant. The distribution of the number of planes N_j for Co and Au layers is given by a discrete distribution about the mean values N_{Co} and N_{Au} with widths s_{Co} and s_{Au}. The lattice spacing is allowed to fluctuate in a continuous Gaussian distribution of width δ about the average lattice spacing d. This δ parameter refers to the quality of the atomic ordering within a single layer and expresses[17] the *intralayer disorder*. The other type of layer disordering that is taken into account from the SUPREX fitting is the *interlayer disorder*. Interlayer disorder refers to the deviation in the periodicity of the layers in the growth direction that results from layer thickness variations and interface disorder. The interface distance h and the interface fluctuation width c parameters are related to the degree of interface (interlayer) disorder. The parameter c refers to continuous interface disorder and its variation with Λ can help to determine whether disorder is localized at the interface[17] or is intrinsic to the layers (intralayer disorder). The fitting parameters were the average number of atomic layers N_{Co} and N_{Au}, the discrete fluctuation widths s_{Co} and s_{Au}, the lattice spacings d_{Co} and d_{Au}, the interface distance h, the interface fluctuation width c, and the scale factor. In this way, the interface layer roughness t_i is determined only from the parameters h and c.

The Co/Au XRD profiles at medium- and high-angle regions are shown in Figs. 2 and 3, respectively. Asymmetric peak intensities are observed below and above the zero-order reflections, that are indexed to (111) and (222) fcc Bragg peaks. Their refinement has been performed in two stages. In the first stage we found that the d_{Au} and the Au layer interface roughness t_i^{Au} remain constant with increasing t_{Co} (or Λ), while the d_{Co} and t_i^{Co} parameters are decreasing. In addition, the parameters h and c exhibit a tendency to increase with increasing t_{Co} (or Λ). The refinement gives the very interesting result that both layers (d_{Co} and d_{Au}) expand relative to the bulk values, with the majority of the low Λ expansion confined to the Co layer.

The main experimental feature is that the d_{111} spacings

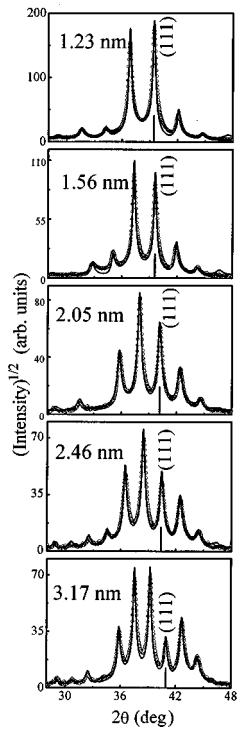

FIG. 2. Plots of medium-angle XRD patterns (points) and the corresponding fitting curves (solid line) obtained from the SUPREX analysis in $[Co(t_{Co})/Au(2.4\ nm)]_{30}$ multilayers. The obtained Co layer thicknesses (t_{Co}) are displayed. The position of the zeroth order reflection, indexed to the (111) fcc Bragg peak, is marked with a bar.

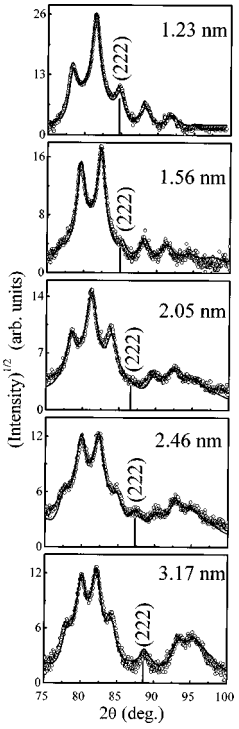

FIG. 3. Plots of high-angle XRD patterns (points) and the corresponding fitting curves (solid line) obtained from the SUPREX analysis in $[Co(t_{Co})/Au(2.4\ nm)]_{30}$ multilayers. The obtained Co layer thicknesses (t_{Co}) are displayed. The position of the zeroth order reflection, indexed to the (222) fcc Bragg peak, is marked with a bar.

for the Co/Au MLs (Fig. 3, top), determined from the position of the fundamental Bragg peak, decrease linearly with increasing t_{Co}. A linear fit (triangular points, Fig. 4, top) of these data gives a $d_{111}(Au)=0.234$ nm for zero t_{Co} that is close to the bulk d spacing of pure Au. Since the d_{111} values provide an out-of-plane lattice parameter averaged over all Co and Au layers in the MLs, this behavior should be reflected in the variation of the d_{Co} and/or d_{Au} parameter. Thus we had to constrain the Co and Au average lattice spacing to follow the observed linear decrease of the d_{111} spacing with increasing t_{Co}. To formulate the linear variation of the lattice spacing as a function of t_{Co} we decided to constrain the interface and intralayer disorder parameters in order to control the changes of the lattice spacing d_{Co} and d_{Au}, and the interface roughness t_i^{Co} and t_i^{Au}.

At the second stage of the SUPREX fitting this behavior is approximated by considering an increase of the interface distance h and the interface fluctuation width c with increasing t_{Co}. The h parameter is constrained to vary between the $(d_{Co}+d_{Au})/2=0.225$ nm value for the thinner Co layer and the $d_{Au}=0.234$ nm limit for the thicker Co layer (Fig. 4, bottom). Also, the interface parameter c was forced to increase linearly with increasing t_{Co} (Fig. 4, bottom). The best fits, with the same fitting parameters in MAS and HAS patterns, are shown with a solid line in Figs. 2 and 3 while their variation is plotted in Fig. 4. Thus, the SUPREX fitting reveals that: (i) The average, out of film plane, d_{111} spacing distances of Co and Au layers are expanded relative to bulk (Fig. 4, top). Thus, the obtained d_{Au} parameter is about 0.237 nm while the d_{Co} values scale linearly between 0.208 and

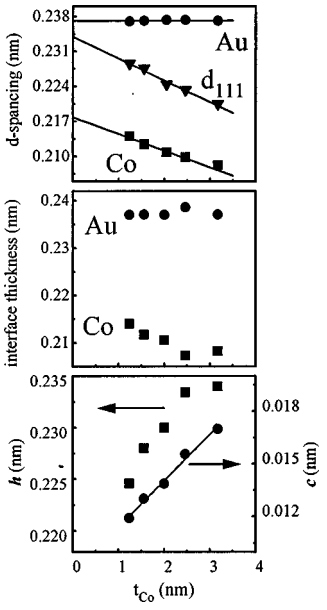

FIG. 4. In $[Co(t_{Co})/Au(2.4\ nm)]_{30}$ multilayers the variation of d_{111} spacings and the obtained lattice spacings d_{Au}, d_{Co} as a function of Co layer thickness t_{Co} is shown on top. In the middle is plotted the variation of the estimated interface roughness t_i for every Co and Au layer. The obtained changes for the interface distance h (left axis) and interface fluctuation width c (right axis) with t_{Co} are shown in the bottom plot. Solid curves are linear fits of the data points.

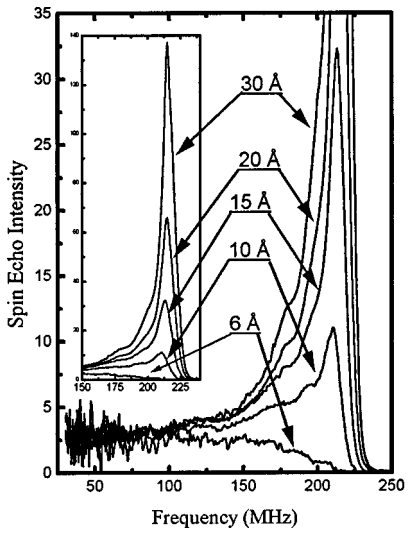

FIG. 5. Spin-echo ^{59}Co NMR spectra in $[\mathrm{Co}(t_{\mathrm{Co}})/\mathrm{Cu}(2.1\ \mathrm{nm})]_{30}$ multilayers with $10<t_{\mathrm{Co}}<35$ nm at 4.2 K. The integral spectra intensity is normalized to the sample area and reflects the intensity variations with Co layer thickness. The frequency range is chosen to present the details of the interface part. The inset shows the details of the bulk part.

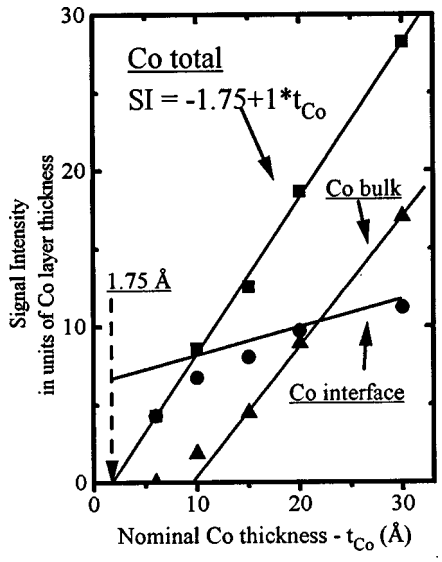

FIG. 6. The variation of signal intensity, obtained from the interface (circles) and bulk (triangles) components of the NMR spectra, is plotted as a function of nominal t_{Co}. The intercept of the extrapolated bulk line indicates that about 1 nm of deposited Co atoms per layer is involved in the interface signal. The plot representing a sum of the bulk and interface signal intensity (squares) extrapolates to zero at about 0.175 nm.

0.214 nm. Comparatively, the corresponding bulk value for fcc Au is $d_{111}(\mathrm{Au})=0.2355$ nm, for hcp Co in the [0001] direction is $d_{0002}(\mathrm{Co})=0.2023$ nm, and for fcc Co is $d_{111}(\mathrm{Co})=0.2047$ nm. The results in Fig. 3 indicate that the strains affect mostly the Co layer structure while the Au layering is unaffected from changes of t_{Co}. The remarkable Co lattice-spacing expansion, that is about 0.04 to 0.1 nm greater than the bulk fcc or hcp Co values, shows that their layer structure is severely truncated along the growth direction. (ii) The obtained interface roughness t_i (Fig. 4, middle) remains unchanged in the Au layer and is equal to the d_{Au} ($\sim$0.237 nm).

IV. NMR SPECTRA OF Co/Cu

In contrast to experimental techniques that measure macroscopic properties, zero-field NMR probes the local magnetic environment of the resonating nuclei through the hyperfine field, $B_{\mathrm{hf}}=(2\pi/\gamma h)A\langle S\rangle$, A and $\langle S\rangle$ being the hyperfine coupling constant and the average electronic spin, respectively. Thus NMR is very sensitive to atoms in the first neighbor shell and probes the local environment—the kind and number of atoms—in the nearest-neighbor (*nn*) shell as well as interatomic distances. It is well established that Co in a regular close-packed environment[18] has the NMR frequency of 217 MHz for the fcc stacking and 220–226 MHz for the hcp. This frequency can be slightly shifted if a strain is present in a sample[19] but a fingerprint of a purely Co environment remains a well-resolved, relatively narrow line. Such a line, corresponding to the ''bulk'' of Co layer, is clearly visible in all the recorded spectra from the Co/Cu MLs with $t_{\mathrm{Co}}\geqslant 1$ nm. The bulk line is fully demonstrated in the inset of Fig. 4, where its frequency position is slightly below the regular nonstrained fcc Co line (212–216 MHz). The lack of structure on the high-frequency side of this peak indicates that there is no significant presence of hcp admixture. According to previous studies[18] we have assumed that each Cu atom introduces a downshift of the NMR frequency by $\sim$16 MHz as a *nn* in a Co host. Thus, the extended tail on the low-frequency side of the main Co line intensity can be assigned to Co atoms located at the Co/Cu interfaces. Figure 5 shows details of the spectrum that exhibit the characteristic features[13] emanating from a Co-Cu interface mixed over several atomic layers.

A coarse estimate of the Co content in the interface region can be made by plotting the variation of signal intensity in the two respective parts of a spectrum with the nominal t_{Co} (Fig. 6). The lower frequency limit for the bulk part was taken at $\sim$205 MHz. The intercept of the extrapolated bulk line indicates that about 1 nm of deposited Co atoms per layer are involved in the interface signal. However, the interface line has a cutoff at a lower value, suggesting that some intensity from the interface is missing due to nonmagnetic or very weakly magnetic fraction of Co atoms. In Fig. 6 the sum of bulk and interface signal intensity extrapolates to zero at about 0.175 nm. This indicates that about one atomic plane of deposited Co per Co layer becomes nonmagnetic. A detailed analysis of the spectra, discussed below, shows that the local Co concentration that is involved in the nonmagnetic interface layers is less than 20%.

Since cross-section TEM images[20] show clearly the Co/Cu multilayer stacking in the columnar grains, a detailed analysis of the interface structure has been performed by assuming symmetric interfaces, using the spectrum modeling procedure described in previous studies.[13,21] In Fig. 7 is shown an example of spectrum decomposition into the hypothetical subspectra computed for each atomic layer in the interface. A bulk Co line can be fitted at 214 MHz (strained fcc Co) as well as a broad line at 205 MHz corresponding to the grain boundaries. The obtained average concentration profile for one bilayer is plotted in Fig. 8 for the sample with

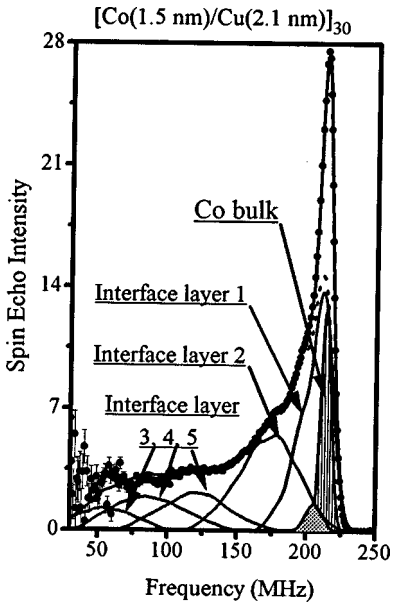

FIG. 7. Experimental and fitted NMR spectrum showing the interface layer contributions and the bulk component (shaded area) from the contribution of the fcc phase. One component corresponding to the grain boundaries is added with a broad line at 205 MHz.

$t_{Co}=1.5$ nm, indicating CoCu intermixing due to interdiffusion at boundaries. However, the absence of a bulk Co signal for $t_{Co}<1$ nm (Fig. 4) shows that Co does not grow in three-dimensional islands (discontinuous layers) because the Co atoms inside the clusters will give rise to bulk Co NMR intensity in the case of island formation.

A closer examination of the spectra in Fig. 5 reveals that with increasing t_{Co} a modification of the interface structure takes place in the frequency range above 150 MHz. This is reflected in the hyperfine field distribution that has been averaged over the entire film volume. To examine this effect, NMR measurements were performed in three Co/Cu samples with different number of bilayers and the same layer thicknesses. As shown in Fig. 9, the relative signal intensity from the interface part of the spectrum is growing larger with the number of bilayers rather than with increasing t_{Co} for constant number of bilayers. Consequently, it may be inferred that an additive Co layer roughness evolves from bottom to top of the Co/Cu MLs due to development of internal stress gradients with increasing film thickness.

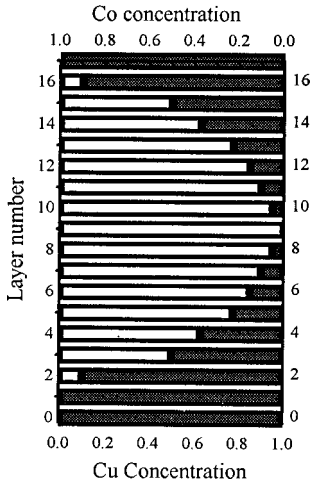

FIG. 8. Average concentration profile for the Co/Cu bilayer obtained from the analysis of the NMR spectrum (Fig. 6) in [Co(1.5 nm)/Cu(2.1 nm)]. The dark levels show the Co percentage per atomic plane.

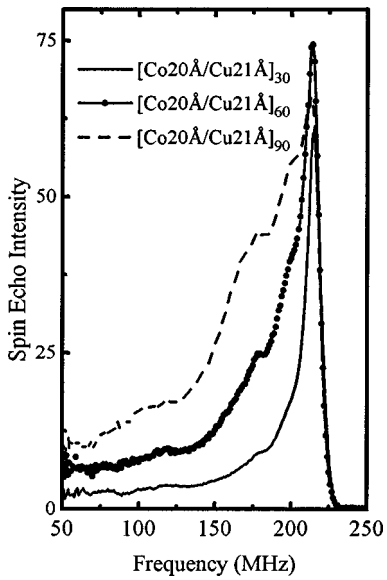

FIG. 9. NMR spectra from three Co/Cu samples with the same Co and Cu layer thicknesses but a different number of bilayers. As shown, the relative signal intensity from the interface part of the spectrum grows significantly as the number of bilayers increases.

V. NMR SPECTRA OF Co/Au AND Co FILMS

In Fig. 10 the Co/Au MLs exhibit totally different NMR spectra from those observed in GMR Co/Cu MLs,[13,21,22] showing one striking feature that is distinct *from all the known* NMR spectra in Co-based MLs. Practically there is no resolved bulk Co line even for t_{Co} as thick as 3 nm. This feature is best displayed in Fig. 11, where the NMR spectra of Co/Au MLs are compared with the corresponding spectra of Co/Cu MLs for $t_{Co}=1$ and 3 nm. Thus is evident that in our Co/Au MLs there is no regular Co environment with 12 Co neighbors located at distances characteristic to the close-packed structures (hcp or fcc). Obviously, a strong modification of the intralayer Co structure has to be introduced in order to explain the large distribution of hyperfine fields in the NMR spectra.

First, it is reasonable to assume that an amorphouslike (topological) disorder can be induced in the Co layers due to large (~15%) lattice mismatch between Co and Au. However, the observed[23] NMR spectra of amorphous Co*M* alloys (*M*=metalloids like B, P, C) exhibit a well resolved Co line, corresponding to Co atoms surrounded only with Co *nn*. The frequency of this line is about 220 MHz, close to that of crystalline Co, and is relatively narrow in contrast to the broad and asymmetric line observed (Fig. 10) in our Co/Au MLs. Thus, a glassy disordering, corresponding to isotropic and homogeneous atomic density of amorphous materials, cannot explain the observed NMR spectra.

A second source of structural disorder may arise from a significant doping (intermixing) of Co layers with: (i) Au

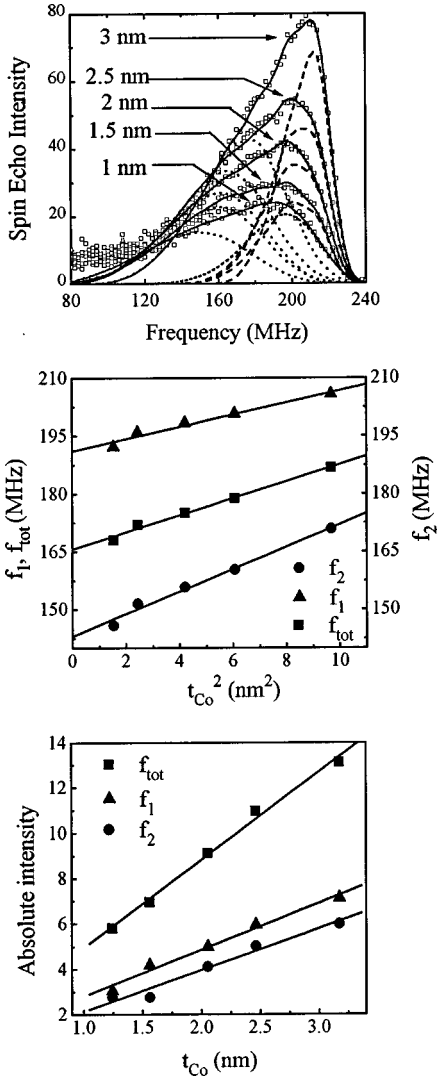

FIG. 10. The experimental (points) and calculated ^{59}Co NMR spectra from $[\mathrm{Co}(t_{\mathrm{Co}})/\mathrm{Au}(2.5\ \mathrm{nm})]_{30}$ multilayers are shown on the top plot. The spin-echo intensity is normalized to the sample area. The obtained frequency positions for the high- (f_1), low- (f_2) frequency zones, and their average frequency (f_{tot}) are plotted in the middle as a function of t_{Co}^2. The integrated intensities for the high- (f_1), low- (f_2), and average frequency (f_{tot}) zones are plotted as a function of the nominal t_{Co} (bottom).

atoms due to interdiffusion and (ii) other impurities (like Co oxides) from a dirty sputtering chamber. To investigate this possibility, we have prepared two Co-rich films under the same deposition conditions: one with a pure Co (60 nm) layer and a second Co (60 nm)/Au (20 nm) film, where the Co layer is protected from oxidation by depositing a Au layer on top. XRD patterns from the as-deposited Co (60 nm) film reveal a broad diffraction feature located (Fig. 12, top) near the fcc and hcp Co Bragg peaks with *Miller* indices (111) and (200). However, in Co (60 nm)/Au (20 nm) the XRD spectra exhibit an intense fcc (111) Au peak and the subsequent (222) fcc peak, indicating that the top layer of Au is (111) textured. Post annealing of the as-deposited Co (60 nm)/Au (20 nm) film at 650 °C for 4 h and of the Co (60 nm) film at 450 °C for 24 h, led to recrystallization of Co layer in the fcc phase (Fig. 12, top). The NMR spectra from the as-deposited and post-annealed Co (60 nm)/Au (20 nm) and Co

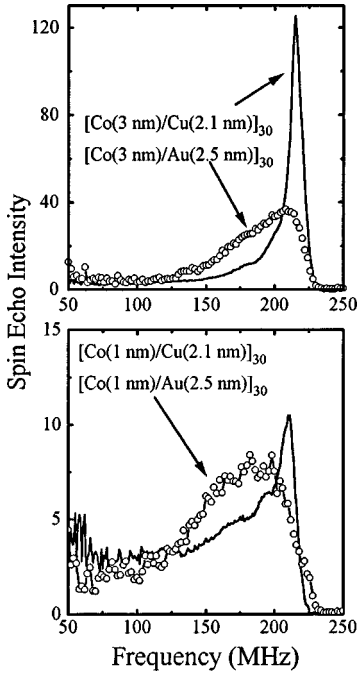

FIG. 11. Comparison of ^{59}Co NMR spectra between Co/Au and Co/Cu MLs with $t_{\mathrm{Co}}=1$ and 3 nm, respectively.

(60 nm) films are shown in Fig. 12. In addition, our XRD data together with previous cross-section TEM measurements[12] provide evidence for a well defined multilayer structure, indicating that an extended doping or Co-Au intermixing is very unlikely.

In this study we consider a structural modification in the Co environment that may reproduce the observed NMR spectra. To fit the NMR spectra a model with two spectral components, later on called ''zones,'' was considered. The component at lower frequencies takes into account the observed intensity from the interfaces, with at least 3 Au *nn*, whereas the bulk Co layer, with 12 Co *nn*, correspond to high-frequency range. The line broadening in every component was approximated by introducing the concept[24] of *magnetic* vacancies. As in Co/Cu MLs, a *magnetic* vacancy at the *nn* shell of Co is assumed to cause a frequency downshift of 16 MHz. The observed line broadening was calculated for every component by considering a random distribution of *magnetic* vacancies in the *nn* shell of Co that produce a binomial distribution of intensities. In this model, the fitting parameters were the *magnetic* vacancy concentration and the relative intensities of the respective spectral components. The agreement between experimental and calculated NMR spectra is shown in Fig. 10 (top).

VI. RELATION BETWEEN HYPERFINE FIELDS AND STRAINS IN Co/Au MLs

The possibility to study the strain of Co with NMR arises from the dependence of the hyperfine field on the atomic distances. Since in Co/Au MLs the linewidth of the bulk Co component broadens significantly by decreasing t_{Co} (Fig. 10, top) then a strain gradient would exist within the Co layer, because the strain induced shift is of the same order as the linewidth.[19] Incoherent Co/Ag and Co/Cu MLs exhibit a[19] shift of the hyperfine field (B_{hf}) with t_{Co} that is proportional

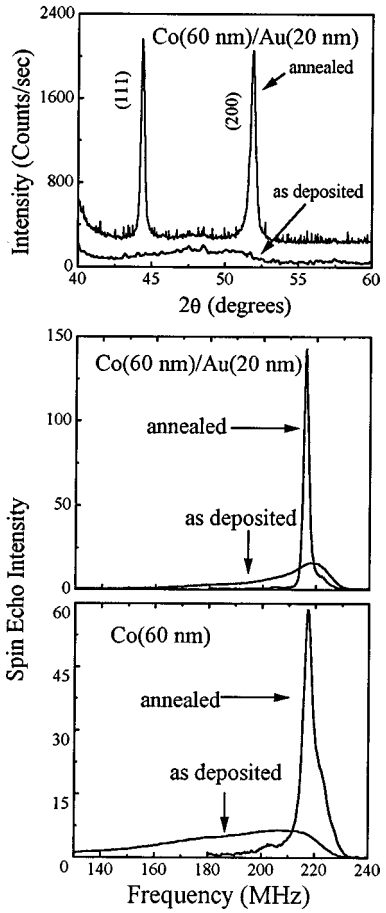

FIG. 12. Typical XRD spectra from the as-deposited and post-annealed Co(60 nm) film are shown on the top. Bottom and middle figures show the NMR spectra from the as-deposited and post-annealed single-layer Co(60 nm) and Co(60 nm)/Au(20 nm) films, respectively.

to the strain (ε) in the interface plane ($B_{\rm hf} \propto \varepsilon$) and inversely proportional to $t_{\rm Co}$ ($B_{\rm hf} \propto 1/t_{\rm Co}$). In our effort to derive a relation between these parameters for the Co/Au MLs, we found that the average frequencies, f_1 (high frequency) and f_2 (low frequency), scale linearly with $t_{\rm Co}^2$ (Fig. 10, middle). Thus the variation of f_1 and f_2 frequencies does not follow the observed[19] $1/t_{\rm Co}$ dependence for completely incoherent MLs.

A tentative explanation for the obtained hyperfine field dependence upon the strain gradient in Co layers is given. Usually, strain gradient in a film is initiated from internal stress variations as we move from the interfaces towards the middle of a layer. Such a case can be realized in a layer-by-layer mode of growth where the film is subjected to a change of interfacial stress from the bottom to the top that causes bending. In a first approximation, the strain is tensile and compressive above and below a *neutral* plane, lying, for example, in the middle of a Co layer. Thus a bulk elastic energy involved in the bending can be calculated by using the common assumption of Euler and Bernoulli[25] where only the normal stress along the direction of curvature is important and the strain ε_{11} and the stress τ_{11} components are symmetric around a *neutral* plane, with $\varepsilon_{11} = (1-\nu^2)\tau_{11}/Y$ (Y is the Young's modulus and ν is the Poisson ratio). The condition for minimum layer curvature correlates the interface stress τ_{11}^s to film thickness t via[26] $\tau_{11}^s \propto Yt^2$, that is valid for all the principal cubic directions (100), (110), and (111) at the interfaces. Thus, the obtained linear variation of f_1 and f_2 frequencies with $t_{\rm Co}^2$ (Fig. 10, middle) indicates that $f_i \propto \tau_{11}^s \propto t_{\rm Co}^2$ ($i=1$ or 2). This result shows that macroscopically *only the normal stress* along the direction of layer curvature is important in our Co/Au MLs. This is consistent with the average lattice expansion obtained along the growth direction from the SUPREX analysis.

VII. DISCUSSION AND CONCLUSIONS

In Fig. 10 the variation of NMR intensity as a function of $t_{\rm Co}$ resembles the dependence of the interface distance h parameter (Fig. 4). This may imply that either the fitted concentration of *magnetic* vacancies originate from *misfit* dislocations at the Co/Au interfaces or excessive internal strain exist along the growth direction of Co. Thus the first one is expected to relieve while the second to increase strain energy in someway for thicker $t_{\rm Co}$. Our ongoing research with cross-section high-resolution (HR TEM) measurements in $[{\rm Co}(1\ {\rm nm})/{\rm Au}\ (2.5\ {\rm nm})]_{30}$ MLs, exhibiting the maximum GMR ratio, reveals an fcc-modulated lattice in every columnar structure of the MLs with numerous {111} twins and stacking faults where, throughout a column, Co and Au form successive layers that grow epitaxially without *misfit* dislocation. These XRD and HR TEM results indicate that the thinner Co layers are excessively stressed and the elastic energy is stored in the lattice, forming a metastable nanostructure.

Comparatively, previous studies[27] indicate that in semicoherent Co/Au(111) interfaces a large concentration of *misfit* dislocations appear inside the entire Co layer volume, whereas Co layers on Ag(111) exhibit *misfits* only near the Co/Ag interface. Also, it was shown[27] that magnetic anisotropy is very sensitive in such kinds of changes at the Co/Au interfaces and the Co layer structure. Furthermore, an NMR study performed[28] in thin Co films grown by molecular beam epitaxy reveals a dependence of the structural phase composition on the substrate and the growth temperature used, which alter significantly the macroscopic magnetic properties. Thus, the strong dependence of magnetization on $t_{\rm Co}$, that is generally observed[29] in ultrathin magnetic layers ($t_{\rm Co} < 3$ nm), does not allow a reliable assignment of a reduced Co magnetization (M_s), relative to bulk Co M_s (~ 1400 emu/cm^3), to be attributed to a certain degree of deformation in Co layers. Conversely, an enhanced M_s (Co) in our samples is out of the question because it would correspond to higher hyperfine fields (frequencies) than that observed in the NMR spectra. Thus in our case a determination of M_s from *typical* magnetic measurements, such as magnetometers or ferromagnetic resonance,[30] cannot provide a unique correspondence to microstructural features.

Alternatively, the conduction made between the average hyperfine field frequencies and normal stresses led to a relation between the strain and $t_{\rm Co}$. In our NMR model the average *magnetic* vacancy concentration, calculated from the high- and low-frequency ''zone'' components, gives an indication about the variation of strain with $t_{\rm Co}$ (Fig. 13). Thus, although the *magnetic* vacancy concentration in both compo-

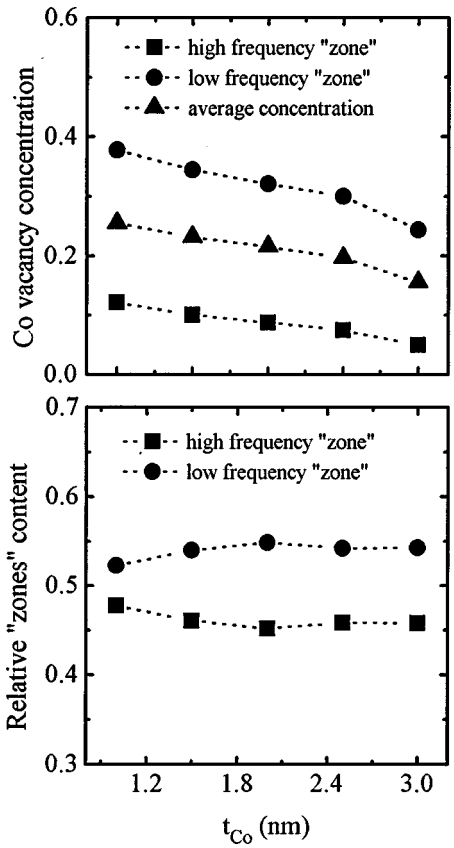

FIG. 13. The average *magnetic* vacancy concentration (triangles), that is calculated from the high- (squares) and low- (circles) frequency zone components, is plotted as a function of t_{Co} (top). The relative zones content that is calculated for the high- (squares) and low- (circles) frequency zone components is shown in the bottom plot.

nents descents by decreasing t_{Co} (Fig. 13, top), the relative volume of the two ''zones,'' calculated as a ratio of the component intensities from the fitting procedure, remains unchanged (Fig. 13, bottom). This result is consistent with a deformed structure where the ratio of bulk to interface *magnetic* vacancy concentrations remains unchanged in the examined t_{Co} region. However, a 10 to 15% average concentration of *magnetic* vacancies inside the Co layers is unusually high and with increasing t_{Co} should lead on formation of line (misfit) or plane (low-angle boundaries) dislocations. In order to investigate the elusive mechanism of strain relaxation in these, low-field GMR, Co/Au MLs additional HR TEM measurements were planned in the near future for the samples with thicker t_{Co} (2 to 3 nm) as well.

In this study, the observed NMR spectra indicate the Co grows pseudomorphically[31] in the fcc phase between the Cu layers, while in our as-prepared Co/Au MLs a metastable nanostructure of Co is generated. Generally, the major difference between the Co/Cu and Co/Au MLs is the lattice mismatch of the constituent elements along the ⟨111⟩ direction of growth. This is about 2% for Co on fcc Cu and about 15% for Co on top of fcc Au. In sputtered Co/Ag MLs that exhibit a 14% lattice mismatch as well it is observed[32] that Ag forms bridges and discontinuous Co layers for $t_{Co}<1.5$ nm. Also, sputter-grown $Ni_{81}Fe_{19}$/Ag MLs[33,34] deposited in temperatures above 300 K and Co layers doped with small amounts[35] of Ag form discontinuous layers and immiscible solid solutions with the Co host, respectively. Conversely, formation of Co-Cu solid solutions[36,37] and metastable phases[38] were reported in thin films and nanocrystalline particles. To the best of our knowledge, formation of substitutional Co-Au solid solutions has not been reported in Co/Au thin films, and the NMR spectra from the as-deposited and annealed Co (60 nm) films exclude this possibility in our Co/Au MLs as well. Since the Co/Cu and Co/Au MLs were grown under exactly the same deposition conditions the deformed Co layer structure in Co/Au MLs can be attributed to the following intrinsic properties: (i) The frequently observed stacking faults in Co films,[39] arising by the negligibly small difference in free energy between the fcc and hcp packing in two dimensions. (ii) The large lattice mismatch between Co and Au. (iii) The unique ability[40] of Au(111) surface to reconstruct during growth of Co layers on Au, which prevent extended diffusion of Au atoms inside the deformed Co layers.

In conclusion, it is demonstrated that structural information obtained from XRD data analysis can be used complementary with ^{59}Co NMR spectroscopy in order to probe indirectly the local structure differences in multilayers with magnetic Co layers. Specifically, while the NMR spectra in our Co/Cu MLs reveal an fcc Co layer stacking, the Co/Au ML's exhibit a broad distribution of magnetic hyperfine fields that cannot be assigned to any of the known crystalline or amorphous Co structures. Analysis of the Co/Au superlattice reflections from the XRD patterns indicates that the Co layers (d_{Co}) expand significantly along the growth direction relative to the close-packed lattice values, with the larger expansion confined to thinner Co layers. This Co layer lattice expansion induce a reduced density and the resultant distribution of internal stresses is reflected in the NMR spectra.

ACKNOWLEDGMENTS

This work was supported by the HTECH.LG 970571-636(97) JARC-412 NATO linkage grant and the EKBAN-280 project of the General Secretariat for Research and Technology of the Development Ministry in Greece. One of the authors, C.C., is indebted to Professor Th. Karakostas for his permission to discuss the HR TEM measurements performed by his group.

[1] N. F. Mott and M. Kaveh, Adv. Phys. **34**, 329 (1985); P. A. Lee and T. V. Ramakrishnan, Rev. Mod. Phys. **57**, 287 (1985); Z. Tesanovic, M. V. Jaric, and S. Maekawa, Phys. Rev. Lett. **57**, 2760 (1986); D. Calecki, Phys. Rev. B **43**, 11 581 (1991).

[2] M. Jalochowski and E. Bauer, Phys. Rev. B **37**, 8622 (1988).

[3] E. Velu, C. Dupas, D. Renard, J. D. Renard, and J. Seiden, Phys. Rev. B **37**, 668 (1988).

[4] V. Grolier, D. Renard, B. Bartelian, P. Beauvillain, C. Chappert, C. Dupas, J. Ferre, M. Galtier, E. Kolb, M. Mulloy, J. P. Renard, and P. Veilet, Phys. Rev. Lett. **71**, 3023 (1993).

[5] Y. Suzuki, T. Katayama, P. Bruno, S. Yuasa, and E. Tamura, Phys. Rev. Lett. **80**, 5200 (1998).
[6] *Ultrathin Magnetic Structures II*, edited by B. Heinrich and J. A. C. Bland (Springer-Verlag, Berlin, 1994), Chaps. 2–4.
[7] S. S. P. Parkin, R. Bhadra, and K. P. Roche, Phys. Rev. Lett. **66**, 2152 (1991).
[8] S. S. P. Parkin and T. Rabedeau, Appl. Phys. Lett. **68**, 1162 (1996).
[9] S. S. P. Parkin, Z. G. Li, and D. J. Smith, Appl. Phys. Lett. **58**, 2710 (1991).
[10] M. J. Hall, B. J. Hickey, M. A. Howson, M. J. Walker, J. Xu, D. Greig, and N. Wiser, Phys. Rev. B **47**, 12 785 (1993).
[11] R. Shad, P. Belien, G. Verbanck, C. D. Potter, H. Fischer, S. Lefebvre, M. Bessiere, V. V. Moshchalkov, and Y. Bruynseraede, Phys. Rev. B **57**, 13 692 (1998).
[12] S. Stavroyiannis, C. Christides, D. Niarchos, Th. Kehagias, Ph. Komninou, and Th. Karakostas, J. Appl. Phys. **84**, 6221 (1998).
[13] C. Meny, P. Panissod, and R. Loloee, Phys. Rev. B **45**, 12 269 (1992).
[14] C. Christides, S. Logothetidis, M. Gioti, S. Stergioudis, S. Stavroyiannis, and D. Niarchos, J. Appl. Phys. **83**, 7757 (1998).
[15] S. Nadolski, M. Wojcik, E. Jedryka, and K. Nesteruk, J. Magn. Magn. Mater. **140-144**, 2187 (1995).
[16] I. K. Schuller, Phys. Rev. Lett. **44**, 1597 (1980); W. Sevenhans, M. Gijs, Y. Bruynseraede, H. Homma, and I. K. Schuller, Phys. Rev. B **34**, 5955 (1986).
[17] E. E. Fullerton, I. K. Schuller, H. Vanderstraeten, and Y. Bruynseraede, Phys. Rev. B **45**, 9292 (1992).
[18] C. Meny, E. Jedryka, and P. Panissod, J. Phys.: Condens. Matter **5**, 1547 (1993).
[19] E. A. M. van Alphen, S. G. E. te Velthuis, H. A. M. de Gronkel, K. Kopinga, and W. J. M. Jong, Phys. Rev. B **49**, 17 336 (1994).
[20] C. Christides, S. Stavroyiannis, N. Boukos, A. Travlos, and D. Niarchos, J. Appl. Phys. **83**, 3724 (1998).
[21] E. Jedryka, M. Wojcik, S. Nadolski, D. J. Kubinski, and H. Holloway, J. Magn. Magn. Mater. **165**, 292 (1997).
[22] P. Pannisod, J. Ph. Jay, C. Meny, M. Wojcik, and E. Jedryka, Hyperfine Interact. **97–98**, 75 (1996); N. Persat, A. Dinia, J. P. Jay, C. Meny, and P. Panissod, J. Magn. Magn. Mater. **164**, 37 (1996).
[23] P. Panissod, A. Qachaou, J. Durand, and H. Hasegawa, Nucl. Instrum. Methods Phys. Res. **199**, 213 (1982); A. Qachaou, Ph.D. thesis, Strasbourg, 1981.
[24] Yu. A. Izyumov and V. Medvedev, *Magnetically Ordered Crystals Containing Impurities* (a special research report translated from Russian consultants bureau).
[25] Chi-The Wang, *Applied Elasticity* (McGraw-Hill, New York, 1953).
[26] H. Ibach, Surf. Sci. Rep. **29**, 193 (1997).
[27] T. Kingetsu and K. Sarai, Phys. Rev. B **48**, 4140 (1993); J. Appl. Phys. **74**, 6308 (1993); **73**, 7622 (1993); T. Kingetsu, Jpn. J. Appl. Phys., Part 2 **36**, L1658 (1997).
[28] H. A. M. de Gronckel, P. J. H. Bloemen, E. A. M. van Alphen, and W. J. M. de Jonge, Phys. Rev. B **49**, 11 327 (1994).
[29] M. S. Cohen, in *Handbook of Thin Film Technology*, edited by L. I. Maissel and R. Glang (McGraw-Hill, New York, 1983), Chap. 17.
[30] Z. Zhang, P. C. Hammel, M. Midzor, M. L. Roukes, and J. R. Childress, Appl. Phys. Lett. **73**, 2036 (1998).
[31] Ch. Rath, J. E. Prieto, S. Muller, R. Miranda, and K. Heinz, Phys. Rev. B **55**, 10 791 (1997).
[32] E. A. M. van Alphen and W. J. M. de Jonge, Phys. Rev. B **51**, 8182 (1995).
[33] M. A. Parker, T. L. Hylton, K. R. Coffey, and J. K. Howard, J. Appl. Phys. **75**, 6382 (1994).
[34] C. Christides, S. Stavroyiannis, and D. Niarchos, J. Appl. Phys. **80**, 4512 (1996).
[35] U. Ebels, R. L. Stamps, L. Zhou, P. E. Wigen, K. Ounadjela, J. Gregg, J. Morkowski, and A. Szajek, Phys. Rev. B **58**, 6367 (1998).
[36] J. R. Childress and C. L. Chien, Phys. Rev. B **43**, 8089 (1991).
[37] C. Gente, M. Oehring, and R. Bormann, Phys. Rev. B **48**, 13 244 (1993).
[38] G. L. Zhou, M. H. Yang, and C. P. Flynn, Phys. Rev. Lett. **77**, 4580 (1996).
[39] H. Lefakis, M. Benaissa, P. Humbert, V. S. Speriosou, J. Werckmann, and B. A. Gurney, J. Magn. Magn. Mater. **154**, 17 (1996).
[40] B. Voigtlander, G. Meyer, and N. M. Amer, Phys. Rev. B **44**, 10 354 (1991).